Synaptic dysregulation in a mouse model of GRIN2D developmental and epileptic encephalopathy

JiaJie Teoh,[1,2] Jane Simko,[1,2] Chad R. Camp,[3] Christine J. Liu,[1,2,4] Wanqi Wang,[1,2,5] Damian Williams,[1,2] Liang Ma,[1,2] Divyalakshmi Soundararajan,[1,2] Caryn Martin,[1,2] Noah K. Taylor,[6] Ekniel François,[1] Sabrina Petri,[1] Ayla Kanber,[1] Aishwarya Ravichandra,[1,2] Maria Elena Pero,[7,8] Francesca Bartolini,[7] Theresa C. Swayne,[7,9] Cathleen M. Lutz,[10] Aamir Zuberi,[10] Moran Rubinstein,[11,12,13,14] Moran Hausman Kedem,[15,16] Hongjie Yuan,[3] Jennifer N. Gelinas,[1,2] Tristan T. Sands,[1,2] Scott Q. Harper,[6,17] Stephen F. Traynelis,[3,18,19] Christopher D. Makinson[1,2,4] and Wayne N. Frankel[1,2,4]

Abstract

Gain-of-function (GoF) variants in the *GRIN2D* gene, encoding the GluN2D subunit of the N-methyl-D-aspartate receptor (NMDAR), cause a severe developmental and epileptic encephalopathy (DEE), characterized by intractable seizures, hypotonia, and neurodevelopmental delay.

We generated mice carrying the GoF V664I variant, orthologous to V667I, which is present in ~25% of *GRIN2D*-DEE patients. Heterozygous mutant mice demonstrate behavioral, neuroanatomical, and electrophysiological abnormalities. Lethal convulsive seizures are observed beginning at postnatal day 17. As adults, heterozygotes display abundant and prolonged runs of spike-wave discharges (SWD) that often persist for minutes. The SWD epochs consist of different populations, differentiated by frequency and association with time-locked behavioral arrest.

V664I mutant neurons have enlarged presynaptic terminals and increased synaptic distance. Functional analysis reveals increased inhibitory synaptic activity without changes in NMDAR decay kinetics or presynaptic plasticity in CA1 neurons and analysis of hippocampal local field potentials show a 1.5-fold increase in evoked responses and a 1.7-fold increase in action potential generation. Notably, expression of V664I in GABAergic interneurons, but not excitatory forebrain neurons, is sufficient to recapitulate the severe electroclinical phenotype.

Altogether our studies show that altered NMDAR function in inhibitory neurons plays a prominent role in DEE associated with *GRIN2D* gain-of-function variants and suggests that targeted genetic treatment may represent a path forward to successful therapeutic intervention.

Author affiliations:

1 Center for Translational Research in Neurodevelopmental Disease in the Department of Neurology, Columbia University Irving Medical Center, New York, NY 10032, USA

2 Department of Neurology, Vagelos College of Physicians and Surgeons, Columbia University Irving Medical Center, New York, NY 10032, USA

3 Department of Pharmacology and Chemical Biology, Emory University School of Medicine, Atlanta, GA 30322, USA

4 Department of Neuroscience, Columbia University, New York, NY 10032, USA

5 Department of Genetics and Development, Columbia University Irving Medical Center, New York, NY 10032, USA

6 Center for Gene Therapy, The Abigail Wexner Research Institute at Nationwide Children's Hospital, Columbus, OH 43205, USA

7 Department of Pathology and Cell Biology, Columbia University Irving Medical Center, New York, NY 10032, USA

8 Department of Veterinary Medicine and Animal Production, University of Naples Federico II, Naples 80137, Italy

9 Confocal and Specialized Microscopy Shared Resource, Herbert Irving Comprehensive Cancer Center, Columbia University Irving Medical Center, New York, NY 10032, USA

10 Rare Disease Translational Center, The Jackson Laboratory, Bar Harbor, ME 04609, USA

11 The Goldschleger Eye Research Institute, Tel Aviv University, Tel Aviv 6997801, Israel

12 The Department of Human Molecular Genetics and Biochemistry, Tel Aviv University, Tel Aviv 6997801, Israel

13 Sagol School of Neuroscience, Tel Aviv University, Tel Aviv 6997801, Israel

14 The Faculty of Medical and Health Sciences, Tel Aviv University, Tel Aviv 6997801, Israel

15 Pediatric Neurology Institute, Dana-Dwek Children's Hospital, Tel Aviv Sourasky Medical Center, Tel Aviv 6423906, Israel

16 The Faculty of Medical and Health Sciences, Tel Aviv University, Tel Aviv 6997801, Israel

17 Department of Pediatrics, The Ohio State University College of Medicine, Columbus, OH 43205, USA

18 Center for Functional Evaluation of Rare Variants, Emory University School of Medicine, Atlanta, GA 30322, USA

19 Center for Neurodegenerative Diseases, Atlanta, GA 30322, USA

Correspondence to: JiaJie Teoh

Center for Translational Research in Neurodevelopmental Disease in the Department of Neurology, Columbia University Irving Medical Center, New York, NY 10032, USA

E-mail: jt3036@cumc.columbia.edu

Running title: Synaptic defects in GRIN2D-DEE mice

Keywords: *GRIN2D*; epilepsy; synaptic dysfunction; neurodevelopment; seizures

Introduction

The N-methyl-D-aspartate receptor (NMDAR) is a heterotetrameric ion channel consisting of two obligatory GluN1 subunits (encoded by the *GRIN1* gene) with two GluN2 subunits (encoded by the *GRIN2A-GRIN2D* genes) or GluN3 subunits (encoded by the *GRIN3A-GRIN3B* genes)[1]. NMDARs are excitatory glutamatergic neurotransmitter receptors that mediate a calcium-permeable current following the binding of both glycine (GluN1/GluN3) and glutamate (GluN2) and coincident membrane depolarization to dispel magnesium ions from within the pore[1]. Thus, NMDARs are key regulators of cellular excitability and, by their capacity to act as coincidence detectors for glutamate release and postsynaptic membrane depolarization, are important synaptic operators for activity-dependent plasticity[2]. Accordingly, impaired NMDARs have been identified in the etiology of diverse neurophysiological behaviors that rely on well-regulated cellular

excitability and synaptic plasticity including cognition[3], synaptogenesis[4] and memory formation[5]. *De novo* missense variants in the *GRIN2A*, *GRIN2B* and *GRIN2D* genes have been associated with developmental epileptic encephalopathy (DEE), a serious form of childhood epilepsy[6]. Furthermore, *GRIN2D* associated DEE is relatively understudied compared to *GRIN2A* and *GRIN2B* disease[7,8].

Among the 22 individuals described with *GRIN2*D DEE to date, 19 (86%) experience seizures with onset ranging from 1 day to 41 months. *GRIN2D* DEE mutations tend to cluster in the NMDAR M3 transmembrane domain[7], including the *GRIN2D* V667I (c.1999G>A, p.Val667Ile) variant, which has been observed in at least 3 individuals[9]. *GRIN2D* V667I patients show developmental delay, hypotonia and speech disorder. Individuals with V667I display a variety of behavioral and electroclinical seizure types, including atypical absence seizure, complex partial seizure, generalized seizure, spike-wave discharges and hypsarrhythmia[8,9]. Anti-seizure drugs are still the mainstay for seizure control, and the clinical response is limited and varies individually[10]. Treatment of *GRIN2D* DEE using memantine, an FDA-approved uncompetitive NMDAR antagonist, was performed in three patients after seizure onsets and achieved varying levels of success[8,9]. To date, no targeted treatment is available for *GRIN2D* DEE.

The V667I variant increases glutamate potency by 1.5-fold, increases channel open probability by 10-fold, and prolongs the deactivation time course 2-fold while simultaneously reducing Mg^{2+} sensitivity by 1.5-fold[9]. These data suggest that *GRIN2D* V667I produces a gain-of-function (GoF) effect. *Grin2d* has been reported in the diencephalon, brainstem, cerebellum, spinal cord, cortex and hippocampus[11]. Detailed studies of cortical and hippocampal *Grin2d* expression in the adult mammalian brain have shown that it is predominantly found in inhibitory neurons[12,13], with lower levels detected in excitatory neurons[11,14,15]. Expression of *Grin2d* begins during embryonic stages, peaks in early postnatal development when it is nearly ubiquitously expressed and is later reduced and refined in the mature brain[16,17]. These raise the possibility that the V667I variant acts to impair different processes in the developing versus adult brain: specifically, embryonic expression leads to disrupted neurodevelopment, while expression in the adult may alter network excitability via a synaptic mechanism involving impairment of inhibition in forebrain circuits.

Here we establish a rodent model of DEE by introducing the *Grin2d*-V664I mutation, orthologous to *GRIN2D*-V667I mutation, documenting behavioral impairments and pronounced seizure phenotypes. *Grin2d*-V664I mutation highlights impaired glutamatergic excitation of inhibitory cells and impaired neuronal inhibition. Informed by these findings, we developed a proof-of-concept precision therapeutic intervention that successfully ameliorates seizure burden observed in the model. Although addressing early-onset intractable DEE in humans presents significant challenges, this study provides valuable insights to guide the future development of innovative gene therapy approaches for children with pathogenic gain-of-function *GRIN2D* variants.

Materials and methods

Mouse strains

The mouse strains used in this study were obtained from The Jackson Laboratory (JAX). These include: C57BL/6J (B6J, Jax #000664), FVB.129P2-*Pde6b*$^{+}$ *Tyr*$^{c\text{-}ch}$/AntJ (FVB.129P2, Jax #004828), B6.Cg-*Edil3*$^{Tg(Sox2\text{-}cre)1Amc}$/J (*Sox2-Cre*, Jax #008454), B6.129S2-*Emx1*$^{tm1(cre)Krj}$/J (*Emx1-Cre*, Jax #005628), B6J.Cg-*Gad2*$^{tm2(cre)Zjh}$/MwarJ (*Gad2-Cre*, Jax #028867), B6.129P2-*Pvalb*$^{tm1(cre)Arbr}$/J (*Pvalb-Cre*, Jax #008069), B6N.Cg-*Sst*$^{tm2.1(cre)Zjh}$/J (*Sst-Cre*, Jax #018973), C57BL/6J-*Grin2d*^{em10Frk}/J (*Grin2d* cKI, Jax #34965) and STOCK *Pde6b*$^{+}$ *Grin2d*^{em9Frk} *Tyr*$^{c\text{-}ch}$/FrkJ (*Grin2d* OT).

Generation of *Grin2d* V664I mutant mice

Grin2d V664I mutant mice were generated in the JAX Center for Precision Genetics (The Jackson Laboratory, Bar Harbor, ME) in the B6J strain using oligonucleotide-directed CRISPR mutagenesis to replace a CG with AA, resulting in a V664I substitution corresponding to the human pathogenic V667I variant. A nonsynonymous A663 substitution introduced a *HypCH4V* restriction site (TGCA) for genotyping. Mice were genotyped using PCR (forward: 5′-AGTATGAGGAGTGGAGGGAC-3′; reverse: 5′-AGCTCCTTTCAGAACCTTCCA-3′), and *Hypch4*V enzyme digestion. *Grin2d* cKI mice were generated using a knockout-first strategywith A loxP-Stop-LoxP V664I knockin cassette inserted between exons 7 and 8 in B6J embryos and founders confirmed by sequencing. . Mutant expression was achieved by crossing with *Cre* driver

strains. Mutant were genotyped using PCR (forward: 5′-GTCCTGTGGGCTATAACCGAAGCC-3′, reverse: 5′- CGTTCAGCTCCTTTCAGAACCTTCCA -3′). Mice were bred at Columbia University's Institute of Comparative Medicine under a 12-h light/dark cycle with ad libitum food and water. 2- to 6-month-old mice were used for mating. All procedures followed Columbia University Irving Medical Center IACUC-approved protocols.

Video-EEG of adult mice and data analysis

Mice (3-4 weeks old, either sex) were given analgesia prior to anesthesia with vaporized isoflurane. Four burr holes was drilled: two bilaterally 1 mm anterior to bregma, one 2 mm posterior on the left, and one over cerebellum as reference. Teflon-coated silver wires (Mouser electronics, 575-501101) were placed between the dura and pia mater, secured with a non-organic dental cap. Postoperatively, mice received additional analgesia and recovered for ≥48 hours before electroencephalography (EEG) recording. EEG was recorded using a Natus Quantum 128 amplifier, with simultaneous video monitoring using a Sony IPELA EP500 camera. Referential traces were obtained between cortical and reference electrodes, resulting in three channels per mouse. Data were acquired in Natus Database v8.5.1.

For power spectra, edf files were preprocessed using MNE-Python by applying a 1-50 Hz bandpass FIR filter. Power spectra were estimated using SciPy's periodogram function with a Hann window at 0.05 Hz intervals up to 50 Hz. Data were normalized to maximum power per channel/mouse using NumPy, saved as text file ajd ajalyzed in JMP 17 (SAS).

For frequency and duration analysis of SWD-like events, ≥25 events were selected based on: (a) immediately prior to the event the video must be evident with the subject exhibiting clear locomotor activity, (b) immediately prior and following the event the EEG must be at baseline level, c) events were drawn from both the light and the dark cycle. The burst fundamental frequency for each event was taken from power spectra using Assyst software's cursor tool (Kaoskey, Inc.) and analyzed in JMP 17 (SAS).

Mouse pup *in vivo* electrophysiology

Pups (P6-P7, P13-P14, either sex) underwent anesthesia induced and maintained with isoflurane. EMG/EKG electrodes were placed subcutaneously in the chest and nuchal areas to monitor heart rate, respiration, and muscle tone. Systemic and local analgesia were administered before head-fixation. A craniotomy (2 mm mediolateral, 3 mm anteroposterior) was perform over the dorsal cortex, exposing multiple regions without damaging the dura. A NeuroGrid array (conformable, biocompatible surface electrocorticography array, 119 electrodes, 177µm pitch) was placed on the brain, with a cerebellar electrode as reference. Pups recovered in a temperature- and humidity-controlled chamber, transitioning into normal sleep-wake cycles. Signals were amplified and digitized at 20 kHz using a RHD2000 head-stage (Intan Technology) and stored in 16-bit format for offline analysis. Data were analyzed using MATLAB (MathWorks) and visualized using Neuroscope. After recording, pups were euthanized for immunostaining.

Local field potential recording

Slices were placed in an interface recording chamber and bath temperature was maintained at 34 ± 1 °C. In some recordings, clonazepam (CZP, 0.2µM) was added to the solution. Neuronal activity was recorded with commercially available linear array probes (Model: A16x1-2mm-100-177, NeuroNexus, Ann Arbor, MI, USA) with 16 contacts (spacing: 100µm distance), spanning 1500 µm. Probes were slowly lowered across the CA3 hippocampus. A bipolar stimulating electrode (World Precision Instruments) was placed across the hilus of the dentate gyrus. Stimulation was delivered at 100µA. Data acquisition was performed through a digitizing board (SI-4, Tucker-Davis Technologies) connected to a real-time acquisition processor (RZ10x, Tucker-Davis Technologies) and PC workstation (WS-8, Tucker-Davis Technologies) running custom-written routines in Synapse (Tucker-Davis Technologies). Recordings were sampled at 24 kHz. Local field potentials were band-pass filtered between 3 and 300 Hz. Multi-unit activity was high-pass filtered between 300-5000Hz. Spikes were recognized at a threshold greater than 5 times the standard deviation of its waveform RMS.

Current source density

Current source density (CSD) analysis was performed to estimate the density of transmembrane current sources. Computations were performed in Python 3.7 using the Elephant 0.7.0 python package, implementing the 1-dimensional electrode set-up kernel current source density method for a non-parametric CSD estimation from arbitrarily distributed electrodes[18]. Cross-validation was performed to prevent over-fitting. CSD data were represented as an $m \times n$ matrix C. Minima values were calculated as the minimum among all datapoints of matrix C with coordinates defined as (m_x, m_y). Current volumes, $Vol(C)$, were calculated as in $Equation$ 1 in which the absolute value of all CSD values in matrix C were summed. Weighted dispersion, $Disp(C)$, was defined as in $Equation$ 2 below as the sum of a weight constant, $|C(x,y)|$, multiplied by a distance from (m_x, m_y), for each iterative coordinate in C.

$$Vol(C) = \sum_{x=0}^{m} \sum_{y=0}^{n} |C(x,y)|$$

Equation 1. CSD Volume

$$Disp(C) = \sum_{x=0}^{m} \sum_{y=0}^{n} |C(x,y)| \sqrt{(m_x - x)^2 + (m_y - y)^2}$$

Equation 2.CSD Weighted Dispersion.

Data visualizations were created using Python Pandas, Scipy, Seaborn, NumpPy and Matplotlib.

RNAi design and luciferase screening assay

Five RNAi candidates were selected from mouse *Grin2d* RNA sequence (CCDS21267.1)[19]. The candidates were designed to also target human *GRIN2D* RNA sequences (CCDS12719.1) with a single nucleotide mismatch that permits the formation of a G-U wobble base pair. Selected candidates were shown below.

miGrin2d-791 corresponds to site 791-812 in RNA.

5'CUCGAGUGAGCGAGCCUGGCUACGUCUGGUUCAUCUGUAAAGCCACAGAUGGGA
UGAACCAGACGUAGCCAGGCCUGCCUACUAGU 3'

miGrin2d-1169 corresponds to site 1169-1190 in RNA.

5'CUCGAGUGAGCGACAGAGACAGGACGUGGGAAGUCUGUAAAGCCACAGAUGGG
ACUUCCCACGUCCUGUCUCUGGUGCCUACUAGU 3'

miGrin2d-1677 corresponds to site 1677-1698 in RNA.

5'CUCGAGUGAGCGAGUCAUGGUGGCACGCAGCAAUCUGUAAAGCCACAGAUGGG
AUUGCUGCGUGCCACCAUGACGUGCCUACUAGU 3'

miGrin2d-2240 corresponds to site 2240-2261 in RNA.

5'CUCGAGUGAGCGAAGGGAAACUGGACGCCUUCAUCUGUAAAGCCACAGAUGGG
AUGAAGGCGUCCAGUUUCCCUGUGCCUACUAGU 3'

miGrin2d-2467 corresponds to site 2467-2488 in RNA.

5'CUCGAGUGAGCGAGGAUCUGCCACAACGACAAAACUGUAAAGCCACAGAUGGGU
UUUGUCGUUGUGGCAGAUCCCUGCCUACUAGU 3'

For candidate screening, the dual luciferase reporter plasmid was modified from Psicheck2 (Promega). It includes a firefly luciferase cassette serving as a transfection control, and the mouse *Grin2d* gene cloned downstream of the *Renilla* luciferase stop codon. HEK293 cells were co-transfected with the luciferase *Grin2d* reporter and each U6.miGrin2d candidate plasmids in a 1:5 molar ratio using Lipofectamine 2000 (Invitrogen, #12566014). *Grin2d* gene silencing was determined as previously described[20]. Triplicate data were averaged per experiment, and individual experiments performed three times. Results were reported as the average ratio of *Renilla* to firefly luciferase activity ± SD for all combined experiments.

RNAi treatment in mice

The miGrin2d-791 sequence was cloned downstream of the U6 promoter, as previously described[20,21] and packaged into a self-complementary AAV serotype-9 vector (scAAV9-NP.U6.miGRIN2D-791, Andelyn Biosciences, #TT1002-1, 5.5 x 10^13 vg/ml). A comparable eGFP control virus (scAAV9-CMV.EGFP, Andelyn Biosciences, #TT900-3, 4.3 x 10^13 vg/ml)

was used. For intracerebroventricular (i.c.v.) delivery, P4 pups were anesthetized by hypothermia, and virus was injected freehand using a 10 µl Neuros Syringe (Hamilton, #65460-06). The injection site was 2mm deep at approximately 2/5 the distance from lambda to each eye. Three miGrin2d-791 doses (5.5 x 10^10 vg, 2.75 x 10^10 vg, and 1.1 x 10^10 vg, in 5 µl) were tested. Control eGFP virus (1.2 x 10^11 vg, in 10 µl) was delivered to pups at P1. Treated pups were maintained under standard breeding conditions.

Quantification of Transduction and Grin2d Knockdown

Forebrains were isolated from miGrin2d-791-treated mice at P14, flash-frozen, and stored at −80°C. RNA was isolated from homogenized tissues using the RNAEasy Mini kit (Qiagen, #74104) according to the manufacturer's instructions. RNA was then converted to cDNA using the SuperScript III first-strand synthesis system (Invitrogen, #18080051). Grin2d knockdown rate was assessed using qPCR with specific primers (5′ -GAGTACGACTGGACATCCTTTG-3′ and 5′ -CAGCACCTCGATGTATGACAAG-3′) and SYBR Select Master Mix (Applied Biosystems, #4472903) on an Applied Biosystems QuantStudio 5. The percentage of Grin2d knockdown was calculated using the comparative CT (ΔΔCT) method.

Automatic SWD quantification

Spikes were detected across the EEG using a NeuroKit2-based algorithm, identifying local maxima exceeding a dynamic threshold. To account for variability, the signal was divided into overlapping windows, and spikes were retained if their amplitudes exceeded the local mean by multiple of the standard deviation. To classify and quantify SWDs, EEG channels were processed using a custom function. A 100,000-sample sliding window computed the mean and standard deviation, filtering spikes that exceeded the adaptive threshold. SWDs were identified by initializing at the first spike and extending the windows (initially 6 seconds) as long as at least six spikes occurs within each six-second segment. The six spikes/six seconds threshold was optimized

by unsupervised learning. Finally, SWDs were classified as either 'Short SWD' or 'Long SWD' based on their duration, with 'Long SWD' defined as those lasting five minutes or more.

Statistical analysis

Statistical methods, sample sizes and p-values are indicated in figure and figure legend of respective results.

Ethical Statement

All analyses were performed as part of clinical care and reported in accordance with Institutional Review Board (IRB) approval. Informed consent was obtained from the parents prior to the inclusion of the patient data.

Additional methodological details are available in the Supplementary Materials.

Results

Generation of V664I mutant mouse models

We developed a mouse model carrying a GoF pathogenic variant in the GluN2D subunit of the NMDAR, causing a non-conservative Val667Ile (V667I) amino acid substitution identified in several children at the severe end of the *GRIN2D* DEE spectrum[8,9]. Two independent mouse lines were generated. Initially oligonucleotide-directed CRISPR/Cas9 mutagenesis was used to replace a CG dinucleotide pair with AA in the C57BL/6J (B6J) mouse strain, resulting in a valine (V) to isoleucine (I) amino acid substitution at the corresponding mouse coordinate, V664 (**Fig. 1A**). Founder mice mosaic for the *Grin2d* V664I mutation were crossed to wildtype B6J mice to obtain heterozygotes. Mendelian transmission of the *Grin2d* V664I/+ genotype was normal prior to weaning (females: +/+, 14 animals; V664I/+, n=14; males: +/+, n=20; V664I/+, n=16). Adult *Grin2d* V664I/+ mice of both sexes are fertile but heterozygotes died as early as 20 days of age.

In efforts to extend the viability of breeders, *Grin2d* V664I/+ were outcrossed to the FVB.129P2 strain, but the lifespan was still truncated in these F_1 hybrid mice.

To provide mice for initial experiments, ovary tissue from these F_1 hybrid mice was transplanted into (FVB.129P2 x B6J) F_1 hosts to generate *Grin2d* ovary-transplanted (OT) breeders. The OT mice were then crossed with FVB/NJ to generate *Grin2d* V664I/+ mutant and wildtype mice. All V664I/+ mutants displayed hindlimb clasping from 2 weeks of age, compared to the normal wide hindlimb splaying of wildtype littermates (**Fig. 1B**), suggesting abnormal motor coordination[22,23].The mutant pups also exhibited delayed growth, with a 1.5 g average difference in body weight by postnatal day 10 (P10, **Fig. 1C**). This observation motivated additional investigation of developmental progression in pups. While developmental milestones including surface righting reflex (**Fig. S1A**), negative geotaxis (**Fig. S1B & S1C**), and ability to hang onto a vertical screen (**Fig. S1D**), shows only modest variations, mutant pups exhibited an increase in maternal separation-associated ultrasonic vocalization (USV) calls, along with a delayed USV peak (**Fig. 1D**). These findings suggest prolonged anxiety and developmental delay. Based on the weight loss observed in mutant pups by P10, comparative histological analysis was conducted between mutant and wildtype littermates at P7 and P14 (**Fig. 1E**). There is no difference in brain size measured as length. (**Fig. S1E**). At both P7 and P14, hypoplasia of thalamus, hypothalamus, striatum and cerebellum were observed (**Fig. S1F, S1G, S1H & S1I**). These findings indicate a developmental delay that may lead to lasting structural abnormalities in the brain.

Given the substantial challenges in maintaining the *Grin2d* V664I/+ mutant line due to premature lethality, we developed a 'knockout-first' conditional knock-in mutation (*Grin2d* cKI, whereby cKI designates the V664I missense allele, and KO or - designates the knockout allele) strategy to facilitate more effective investigation of *Grin2d*-V664I phenotypes (**Fig. 1F**). Knockout-first homozygous mice are *Grin2d*$^{-/-}$ and the heterozygous mice are *Grin2d*$^{+/-}$. Both mice are fertile, lack overt abnormal behaviors, and have lifespan comparable to wildtype mice. *Grin2d* cKI (*Grin2d*$^{-/-}$ or *Grin2d*$^{+/-}$) mice were crossed to a *Sox2-Cre* driver strain to introduce the V664I mutation broadly throughout the brain by targeting Sox2-expressing neural progenitor cells, which then give rise to various neural cell types. This approach effectively mimics the widespread nature of the germline mutation found in patients. *Sox2-Cre* V664I/+ mice were found to have elevated expression of GluN2D in the forebrain (**Fig. 1G & 1H**) and an intermediate survival phenotype (~50%) as compared to the OT model by P60 (**Fig. 1I,** dotted line).

Developmental and cell type-specific consequences to seizure phenotypes of Grin2d-V664I

Grin2d is known to be expressed broadly in the brain, particularly during early development[12,13]. To explore the contribution of individual genetically specified neuronal cell types to V664I-associated phenotypes, *Grin2d* cKI mice were crossed to five different cell type-specific *Cre*-driver strains: *Gad2-Cre* (all GABAergic neurons), *Pvalb-Cre* and *Sst-Cre* (subsets of GABAergic neurons), *Emx1-Cre* (forebrain glutamatergic neurons), or *Sox2-Cre* (broad expression). In addition, heterozygous *GRIN2D* (*Grin2d*$^{+/-}$) and wildtype B6J (*Grin2d*$^{+/+}$) mice were included for comparison.

Grin2d$^{+/-}$ and wildtype mice did not exhibit hindlimb clasping phenotype (**Fig. 1b**). Furthermore, the survival of *Grin2d*$^{+/-}$ mice (100% at P60, N=13) was comparable to wildtype mice (100% at P60, N=11). Therefore, they were grouped as controls in subsequent experiments. Among the neuron subclass-specific models, only *Gad2-Cre* mutants resulted in lethality. The lethality rate is 100% by P31 with median survival occurring even earlier than in the broad targeting *Sox2-Cre* mutants (**Fig. 1I & 1J**). In contrast, all *Emx1-Cre* mutants survive to P31, comparable to the control group. Interestingly, the survival of *Gad2;Emx1* double-*Cre* mutants closely mirrored that of *Sox2-Cre* mutants, with 67% survival at P31 compared to 64% for *Sox2-Cre* mutants (**Fig. 1J**), showing no significant difference (p=0.54, Kaplan Meier's log-rank test). These results point to a partial ameliorative effect on survival of introducing the V664I mutation to excitatory neurons. Consistent with these results, cleaved Caspase-3 immunostaining showed significant cell death in the rostral migratory stream (RMS) and hippocampus of P16 *Gad2-Cre* mutant brains. In contrast, minimal cell death was observed in the *Emx1-Cre* mutants, *Sox2-Cre* mutants, and wildtype brains (**Fig. 1K & 1L**). RMS contains neuroblasts migrating from subventricular zone to become inhibitory neurons in the olfactory bulb within the first three postnatal weeks[24,25] . This indicates that V664I expression in Gad2^{+} neurons interferes with neuronal differentiation and survival within the RMS. Partial restoration of these phenotypes by the *Emx1-Cre* allele, however, did not extend to hindlimb clasping, as *Gad2-Cre*, and *Gad2;Emx1* double *Cre* mutant mice both displayed hindlimb clasping behavior[26]. Like *Emx1-Cre* mice, no sign of premature death was observed in *Pvalb-Cre* and *Sst-Cre* mutants up to P31.

Most *Sox2-Cre* mutant carcasses, like those of OT V664I/+ mutants, were found with forelimbs and hindlimbs extended, indicating that lethality was due to severe tonic-clonic seizures. To further characterize putative seizures, in-depth video electroencephalography (vEEG) was performed. Prominent epileptiform activity was observed, including multiple seizure types, in both OT and *Sox2-Cre* V664I/+ mutants, but not in *Grin2d* $^{+/-}$ or wildtype mice (**Fig. 2A & 2B**). Many events were reminiscent of spike-wave discharges (SWDs) like those observed in absence epilepsy mouse models[27]. Rodent SWD events, typically last for several seconds[28]. However, V664I/+ mutant mice display prolonged SWD events, persisting in many cases for minutes. These SWD-like events, with the fundamental frequency ranging from approximately 5 Hz to 9 Hz, were heterogeneous in appearance and frequency and observed at all adult ages examined (**Table 1**). Interestingly, at least one child with the V667I mutation exhibited similar SWD-like electroclinical features (**Fig. S2).** Lethal tonic-clonic seizures were captured in five animals during these recording sessions (**Fig. 2C**), supporting the conclusion that such seizures contribute to premature lethality in these models.

Although vEEG could not be recorded from *Gad2-Cre* mutants due to complications related to early lethality, distinct differences in SWD activity were observed following V664I activation in different inhibitory neuron subtypes. Expression in *Pvalb*+ neurons (**Fig. 2D)** led to relatively high fundamental frequency and amplitude of SWD-like events in all mice examined whereas among *Sst-Cre* mutants (**Fig. S3A)**, only a few animals displayed SWD and these events were significantly shorter in duration and less frequent, resembling typical SWD events described in other models[28]. By contrast, *Emx1-Cre* mutants (**Fig. S3B)** had no evident abnormal EEG activity.

Prompted by these observations, we analyzed the EEG normalized power spectra to compare *Sox2-Cre*, *Pvalb-Cre*, *Emx1-Cre* mutants and control *Grin2d*$^{+/-}$ and *Grin2d*$^{+/+}$ mice across relevant frequency ranges (**Fig. 2E & 2F**). Pairwise analysis reveals profound differences between the epileptic mutants and controls, particularly in the 4 Hz-7 Hz and 7 Hz-10 Hz range, and between *Sox2-Cre* and *Pvalb-Cre* in the latter band. By contrast, the power spectrum of *Emx1-Cre* mutants was comparable to wildtype *Grin2d*$^{+/+}$.

Behavioral arrest was observed during SWD events in *Pvalb-Cre* cKI animals, as expected for SWD events in mice resembling typical absence epilepsy. However, we noticed that the electrographic-behavioral association was more heterogeneous in *Sox2-Cre* mutant mice, in which ongoing motor behaviors were not always interrupted by SWD-like activity. Further examination

of the EEG and motor behavior revealed that the events associated with continued motor activity had a significantly higher fundamental frequency and shorter average duration than those that interrupted behavior (**Fig. 3A & 3B**). Notably, while SWD-like events in *Pvalb-Cre* mutants always interrupted ongoing locomotor activity, the fundamental frequency was also high (8.1 Hz ± 0.05 SE). On average, the events associated with behavioral arrest were significantly longer than those did not involve behavioral arrest. Collectively, these analyses indicate that subtypes of electroclinical events are associated with the impairment of different interneuron subtypes in V664I-DEE.

Grin2d expression in mice begins embryonically and is down-regulated gradually over the first postnatal week[16,17,29]. To investigate electrographic activity during this dynamic early postnatal period, we conducted acute, head-fixed, unanesthetized, *in vivo* electrocorticography on *Sox2-Cre* V664I/+ pups and littermate controls (*Grin2d*$^{+/-}$), at P6-P7 and P13-P14. A soft and conformable dense electrode array was used to sample network activity from a large continuous area of the dorsal cortical surface **(Fig. 3C, white dotted box)**. Cortical activity patterns were similar between *Sox2-Cre* V664I/+ and *Grin2d*$^{+/-}$ control pups at the end of the first postnatal week (P6-P7) **(Fig. 3D)**. However, by the end of the second postnatal week (P13-P14), epileptic bursts were observed in *Sox2-Cre* V664I/+ mice **(Fig. 3E)**, featuring a notably sustained period of continuous epileptic activity **(Video S1)**. These results suggest that epileptic activity emerges in *Grin2d* V664/+ mice as early as the second postnatal week in mice, coinciding with the refinement of broad early life *Grin2d* expression to adult expression patterns[17].

Impaired synapse structure in V664I hippocampal neurons

Prior work has demonstrated that transfection of *Grin2d*-V667I into cultured neurons induces dendritic swelling[9]. In cultured V664I/+ primary hippocampal neurons, co-staining with the presynaptic marker bassoon and the postsynaptic marker homer 1b/c as well as the synaptic vesicle marker synaptophysin confirmed the presence of atypical dendritic swelling, characterized by enlarged synaptophysin puncta along the proximal dendrites (**Fig. 4A**). Under confocal microscopy, the pre- and postsynaptic markers exhibited irregular and loosely distributed pre-post synaptic associations. In contrast, control cultured neurons showed the expected alignment of presynaptic, synaptic vesicles, and postsynaptic compartments along proximal dendrites. Further

quantification revealed that the density of wildtype-sized synaptic puncta - smaller than 1 µm – showed no significant difference in density, while enlarged synaptic puncta - greater than 2.5 µm - were more abundant along V664I/+ dendrites compared to control (**Fig. 4B & 4C**). To gain a better understanding of the morphology of synapses on cultured primary hippocampal neurons, we performed super resolution STORM imaging. The analysis revealed that the large synaptic puncta in V664I/+ neurons corresponded to a single enlarged synapse, characterized by an enlarged presynaptic compartment with a normally sized postsynaptic compartment, spanning a wider synaptic cleft (**Fig. 4D & 4E**). In V664I/+ hippocampal slices, immunostaining revealed large synaptophysin puncta localized in the CA3 *stratum pyramidal*e (SP) together with a reduction of synaptophysin puncta in the *stratum radiatum* (SR) (**Fig. 4F & 4G**). This suggests a shift in the distribution of synaptic vesicles across hippocampal layers. Additionally, larger synaptic vesicles were found to increase in the CA1 SR layer (**Fig. 4F & 4H**). These changes, however, did not affect dendrite branching in cultured *Sox2-cre* V664I/+ hippocampal and cortical neurons (**Fig. S4A, S4B, S4C & S4D**). Although dendrite branching was not affected, we hypothesized that these changes in dendritic and synaptic morphology would still correlate with impairment in synaptic and neuronal circuit function.

Synaptic and circuit dysfunction in the mutant hippocampus

To better understand the functional changes resulting from the *Grin2d*-V664I mutation, electrophysiological analysis of synaptic and intrinsic excitability was performed on hippocampal slices. To test whether the GoF mutant subunit functionally participates in synaptic transmission, we measured pharmacologically-isolated electrically-evoked NMDAR currents in CA1 excitatory and inhibitory neurons. We observed no genotype difference in weighted time constant (tau) associated with the decay phase of the postsynaptic current in both CA1 excitatory and inhibitory neurons (**Fig. 5A**). These results suggest that the V664I mutation does not significantly alter the postsynaptic decay kinetics of NMDAR currents in CA1 neurons, regardless of cell type.

Given that the V664I mutation does not change the decay kinetics of NMDAR currents, we next examined whether inhibitory synaptic outputs were affected by analyzing spontaneous and miniature postsynaptic inhibitory currents (sIPSCs/mIPSCs) in CA1 excitatory neurons. We observed a notable increase in the frequency of sIPSCs, as indicated by a leftward shift in the inter-

event interval accompanied by a reduction in the sIPSC amplitude (**Fig. 5B**). Similarly, a significant leftward shift in the inter-event interval of mIPSCs was observed, although the mIPSC amplitude remained unaltered (**Fig. 5C**). These findings suggest that elevated inhibitory tone in V664I mutant mice occurs independently of changes in NMDAR decay kinetics.

Seizure has been associated with an increase in the ratio of synaptic excitation (E) and inhibition (I), though this relationship is complex and depends on both brain state and circuit[30]. To estimate E:I ratio, synaptic conductance decomposition was performed of evoked synaptic currents in V664I/+ hippocampal neurons (**Fig. S5A & B**). Synaptic current recordings from CA3 neurons were used to decompose excitatory and inhibitory conductance components as previously described[31]. The reversal potential (E_{rev}), total synaptic conductance (G_{Total}), and the ratio of excitatory to inhibitory conductance (G_{exc}/G_{inh}) showed no significant differences between V664I/+ and control CA3 neurons (**Fig. S5A & B**). These findings suggest that the V664I mutation does not disrupt the balance of evoked excitatory and inhibitory synaptic transmission, despite alterations in spontaneous synaptic events.

Given the lack of differences in postsynaptic NMDAR decay kinetics and the increase inhibitory tone observed in CA1 excitatory neurons, we next evaluated presynaptic function by performing paired-pulse ratios (PPR) experiments[32] in both cortical L5 and hippocampal CA3 neurons. However, we found no significant differences in PPR across all conditions (**Fig. S5C & S5D**), indicating that the V664I mutation does not impact short-term presynaptic plasticity. To further confirm the contribution of Grin2d-containing NMDARs, we conducted control recordings in the presence of NAB-14, a GluN2C/D-specific inhibitor **(Fig. S5E & S5F**). Consistent with the absence of PPR differences, NAB-14 application did not reveal a genotype-specific effect on presynaptic function. These findings suggest that the elevated inhibitory tone observed in CA1 neurons is unlikely to result from altered presynaptic release properties and instead reflects changes in inhibitory network activity downstream of the mutation.

To investigate the consequences of the V664I mutation at the circuit level in the hippocampus, we prepared acute slices preserving the connectivity between the dentate gyrus (DG) and CA3 regions. Local field potentials (LFPs) were recorded using linear 16-channel silicon electrode arrays spanning the CA3 pyramidal layer, while a bipolar electrode delivered stimulation within the hilus (**Fig. 6A**). LFP analysis revealed enhanced excitatory synaptic activity and prolonged current sinks

in the V664I/+ mutant CA3 SR, as indicated by persistent current sinks (region flanked by white dotted lines, **Fig. 6B)**. Mutant slices exhibited larger current volumes, greater current dispersions and lower current minima (**Fig. 6C**), indicating a more intense and spatially widespread circuit response compared to control slices. To assess the contribution of synaptic inhibition in this elevated network activity, we applied clonazepam (CZP, 0.2 µM), a $GABA_A$ receptor enhancer[33], to both V664I/+ and control slices. As expected, CZP suppressed current sinks in control slices. However, in mutant slices, CZP was unable to reduce the amplitude of current sinks (**Fig. 6D,** region flanked by white dotted lines). Moreover, current volume, dispersion and minima significantly increased compared to baseline (**Fig. 6E**), suggesting that despite CZP enhanced $GABA_A$ receptor potentiation, neural activity in the mutant CA3 SR remains abnormally elevated.

Analysis of multiunit activity showed significant differences between V664I/+ and control slices. In V664I/+ mutants, the immediate response to electrical stimulation, measured as action potentials generated by monosynaptic activation within the first 50 ms, was significantly elevated compared to controls (**Fig. 6F**), as reflected in increased spike frequency and counts (**Fig. 6G & 6H**). Surprisingly, V664I/+ slices exhibited lower resting spike count during the 50-200 ms period following the initial stimulus-evoked burst (**Fig. 6F**) where its spike counts were significantly lower than the control (**Fig. 6H**). Given the increase spike frequency within the first 50 ms in the mutant slices, we continued to assess the impact of enhancing GABAergic inhibition on spike activity. Application of 0.2 µM CZP to the perfused extracellular solution reduced spike within the first 50 ms post-stimulation in the control CA3-DG circuit (**Fig. 6I**). Although CZP treatment noticeably decreased overall spike counts in the mutant CA3-DG circuit, the spike counts and frequency within the first 50 ms post-stimulation remained higher in mutants compared to controls (CZP vs untreated, 2.72±0.34 vs 4.12±0.34) (**Fig. 6J & 6K)**. In contrast, spike counts during 50-200 ms post-stimulation were comparable between mutants and controls (**Fig. 6K**). These findings point to altered inhibitory regulation in V664I/+ hippocampal network, leading to hyperexcitable responses to stimuli but reduced baseline activity.

RNAi treatment reduces V664I seizure burden

Previous studies have demonstrated that even complete loss of GluN2D function results in much milder phenotypes[7] compared to those observed in V664I/+ mice. Based on this, we hypothesized

that reducing GluN2D function via RNA interference (RNAi) in the brain of neonatal V664I/+ mice could be a viable strategy to mitigate associated pathological features. To test this, we adapted a previously described strategy[34], using a self-complementary adeno-associated virus serotype 9 (scAAV9) to deliver a small artificial miRNA targeting *Grin2d* mRNA, via i.c.v. injection into neonatal pups at P4. Five miRNA candidates were designed, with *in vitro* screening identifying miGrin2d-791 as the most effective, achieving a 61% knockdown (**Fig. 7A**). This candidate was selected for *in vivo* evaluation at three doses: high (5.5 x 10^10 vg), mid (2.75 x 10^10 vg), and low (1.1 x 10^10 vg).

All treated V664I/+ mice showed improved post-weaning body weight compared to untreated V664I/+ mice (**Fig. S6A**). Survival was significantly extended in the mid and low dose groups, whereas the high-dose group did not exhibit this improvement (**Fig. S6B**). RNA knockdown rates were 69%, 76% and 57% for the high, mid, and low doses, respectively (**Fig. 7B**), suggesting that while *Grin2d* KO mice being viable[35], there may be an upper tolerance limit for miGrin2d-791 that could knockdown both wildtype and V664I GluN2D. EEG recordings revealed that the power spectra of mid-dose treated V664I/+ mice shifted toward the control (wildtypes and *Grin2d*$^{+/-}$) levels, whereas the low-dose group remained similar to untreated V664I/+ mice (**Fig. 7C**). The most pronounced effect of mid-dose treatment was observed in the 4 – 7 Hz range (**Fig. 7D**). Additionally, mid-dose treated animals exhibited shorter SWDs (**Fig. 7E**). Automated quantification showed significant reductions in both SWD duration and the percentage in mid-dose treated V664I/+ mice (**Fig. 7F**), with a 26.5% reduction in the total recording time spent in SWDs and an approximate 30-second decrease in average SWD length compared to untreated V664I/+ mice (**Fig. 7G & 7H**). These results indicate that precisely controlling *Grin2d* knockdown within an optimal therapeutic window may effectively reduce seizure activity.

Discussion

We present a novel *GRIN2D*-DEE mouse model carrying a GoF V667I variant, identified in at least three children[8,9] among 14 pathogenic *GRIN2D* variants in ClinVar. The orthologous V664I mutation in mice produces robust and consistent phenotypes across genetic backgrounds, closely aligning with clinical observations. Notably, this model displays severe seizures, unlike many rodent epilepsy models which often do not replicate prolonged seizure as observed in patients[8-10]. EEG recordings show frequent, complex SWD activity and terminal tonic-clonic seizures,

alongside developmental phenotypes including growth delay, altered USV call frequency and early epileptiform activity – all features seen in affected children[7]. These findings emphasize the model's unique relevance for *GRIN2D*-DEE research (See also Yam et al. accompanying submission).

Although direct comparisons to human electroclinical findings are challenging, high-amplitude theta activity (5-8 Hz) recorded during sleep EEG in a V667I patient (**Fig. S2**) closely resembles a key feature of our model. Similar abnormal high-voltage theta frequency activity has also been reported in the sleep EEG of a patient with another heterozygous *de novo GRIN2D* variant, M681I[36], which, like V667I, is located in the M3 domain and expected to produce GoF effects, though it has not been functionally characterized[8]. Whether this abnormal theta frequency activity signifies enhanced channel function or could serve as a potential biomarker in future clinical trials for *GRIN2D* DEE remains to be determined.

Genetic dissection of *Grin2d*-V664I in specific cell types provided important insights into the mechanisms governing neurophysiological and behavioral phenotypes of *GRIN2D*-DEE. *Grin2d*-V664I expression was induced using constitutive OT model and *Sox2-Cre* for conditional activation. Brain-wide expression was required to produce locomotor phenotypes and complex SWD activity. Inhibitory neuron-specific expression of *Grin2d*-V664I was sufficient to induce spontaneous seizures, including SWD and tonic-clonic seizures. The GABA in the mouse cortex switches from depolarizing to hyperpolarizing around the second postnatal week[37]. The mortality of *Gad2-Cre* mutants that occurred shortly after this developmental period may significantly contribute to triggering lethal seizures in *GRIN2D*-DEE. Among the inhibitory *Cre* drivers tested to introduce V664I, *Gad2-Cre* targeted inhibitory neurons from both the medial ganglionic eminence (MGE) and caudal ganglionic eminence (CGE), while *Pvalb-Cre* and *Sst-Cre* targeted classes of inhibitory neurons originating from the MGE[38]. Based on these findings, our study emphasizes the critical role of precise neuronal targeting in elucidating the pathophysiology of *GRIN2D*-DEE and highlights potential avenues for targeted therapeutic interventions.

Because the selected interneuron *Cre* drivers activate late in development yet are capable of inducing spontaneous seizures, we conclude that at least some seizure phenotypes are driven by ongoing effects of V664I on neuronal excitability rather than a residual consequence of any early developmental impairment. While in the adult brain, *GRIN2D* is predominantly expressed within

inhibitory neurons[13,39], the expression has been reported in excitatory neurons[40], which motivated an evaluation of excitatory cell-specific expression of *Grin2d*-V664I. However, no appreciable behavioral or EEG phenotypes were observed in mice with selective expression of *Grin2d* V664I in excitatory neurons via *Emx1–Cre*. We acknowledge that *Emx1* is highly restricted to excitatory neurons and astrocytes of the cortex, hippocampus, and basal ganglia[41], and is absent in the majority of excitatory neurons in the midbrain or thalamus, where *Grin2d* expression is significant. Future studies examining the role of *GRIN2D* in seizure behaviors involving these regions may be warranted. Pan-neuronal expression of *Grin2d* V664I is, in principle, most equivalent to the human condition[7], and together with *Gad2;Emx1* double-*Cre*, they are the only mouse genotypic contexts that resulted in a consistent hindlimb clasping phenotype. The ameliorating effect of Emx1 in the context of *Gad2;Emx1* double-*Cre* is intriguing and was also reported in Dravet syndrome[42]. These results point to complex combinatorial involvement of V664I/+ in excitatory neurons and inhibitory neurons in the pathogenesis of phenotypes.

The observed brain hypoplasia from P7 to P14 in heterozygous *Grin2d* V664I matches the spatial and temporal expression pattern of the gene in mouse brain[17]. The absence of significant cell death during this period implicates factors beyond neuronal loss, such as white matter shrinkage or possibly agenesis. Hyperexcitation of NMDARs is known to cause myelination loss and axonal damage[43,44]. Notably, the reduction in size observed in white matter-rich regions such as the striatum, a crucial area for gating axon tracts of the cortico-thalamocortical loop, may reflect impaired reciprocal network activation between the cortex and thalamus, which is a key circuit involved in the generation of SWDs[45].

Enlarged synaptic puncta, similar to those observed along the dendrites of cultured neurons overexpressing *Grin2d*-V667I[9], were identified in cultured primary neurons and hippocampal sections. A study of *Disc1* mutant mice that previously reported a similar hippocampal phenotype characterized by errors in axonal targeting and changes in short-term plasticity of local circuits[46], may provide insights into the *Grin2d* V664I model. Within the enlarged synapses of *Grin2d* V664I/+ primary hippocampal neurons, we observed a lack of closely packed synaptic vesicles, which comprise the reserve and readily releasable synaptic vesicle pools. While further interrogation is necessary, this observation, along with our finding of altered PPR point to altered synaptic vesicle recycling in *Grin2d*-V667I animals.

Our findings reveal that enhancing $GABA_A$ receptor function with CZP failed to suppress network hyperexcitability in V664I/+ slices and instead redistributed activity over a prolonged period. While CZP effectively reduced early post-stimulation spiking in control slices, it did not normalize mutant excitability, suggesting that inhibitory dysfunction in V664I/+ circuits is not due to a simple loss of GABAergic signaling but rather a disruption in the timing and efficacy of inhibition. This observation highlights a potential limitation of traditional anti-seizure medications that broadly enhance inhibition but do not correct the underlying NMDA receptor dysfunction caused by the GRIN2D mutation. The paradoxical effects of clonazepam suggest that pharmacological approaches targeting downstream circuit activity may be insufficient for *GRIN2D* V667I DEE.

Given this limitation, a gene therapy that could rescue excitatory-inhibitory balance at its source, preventing circuit-level hyperexcitability rather than merely attempting to suppress downstream effects is a more targeted therapeutic approach. We investigated *Grin2d* RNAi gene therapy as a targeted approach to mitigate disease phenotypes. Our findings indicate that partial knockdown of *Grin2d* effectively improved key disease outcomes in V664I/+ mice, including body weight, survival, and seizure burden. Notably, an intermediate dose of mi*Grin2d*-791 yielded the most favorable outcomes, suggesting an optimal therapeutic window that balances efficacy and safety. Our current RNAi construct achieved a 26.5% reduction in seizure burden and we believe there is significant potential for further optimization, for instance, by incorporating an inhibitory neuron-specific promoter into the RNAi construct, as suggested by the enhanced seizure phenotype observed in the inhibitory neuron specific mutants. However, the absence of improved survival with the high dose may indicate dose-dependent toxicity, potentially linked to the knockdown of wildtype GluN2D or the critical changes in *Grin2d* expression during the first postnatal week[17].

These findings underscore the potential of mutation-specific gene therapy for GRIN2D-related DEE, where targeted RNAi knockdown of the mutant allele could provide a more precise and effective treatment than conventional pharmacological interventions. Future studies optimizing RNAi delivery, dosing strategies, and long-term effects will be crucial in advancing Grin2d-targeted therapies toward clinical translation.

A persistent limitation of rodent models of DEEs is that the associated disease phenotypes are typically mild, especially regarding electroclinical features, when compared to their human counterparts[47]. In this study, we present a rodent model of DEE that exhibits unusually severe and

complex seizure phenotypes, both behaviorally and electroclinically. Our mouse model of *GRIN2D*-DEE, which carries the V664I mutation, demonstrates robust and clinically relevant phenotypes, making it a valuable platform for investigating disease mechanisms and therapeutic development. Detailed characterization of genetic, developmental, and neuronal-specific effects revealed cellular, synaptic and circuit impairments that collectively contribute to the neurophysiological and behavioral phenotypes *in vivo*. Overall, this model represents a significant advancement in the study of DEE, further bridging the gap between rodent models and human clinical manifestations.

Data availability

The data that support the findings of this study are available from the corresponding author upon reasonable request.

Funding

This work was supported by grants from the National Institutes of Health NIH: F31 NS113530 to C.R.C., R35 NS111619 to S.F.T., R01 NS031348 to W.N.F., R21 NS121980 to C.D.M. and W.N.F., U54 OD020351 to W.N.F., R01 HD082373 to H.Y., RF1 AG050658-01 to F.B. and a BSF grant to W.N.F., C.D.M. and M.R.. J.S. was supported by the NIH BRAIN Initiative grant F32 MH130023. C.J.L. was supported by the National Science Foundation Graduate Research Fellowships Program (GRFP) DGE-2036197. S.F.T. was also supported by the Simon's Foundation. These studies used the resources of the Herbert Irving Comprehensive Cancer Center Confocal and Specialized Microscopy Shared Resource, funded in part through NIH/NCI Cancer Center Support Grant P30CA013696 and the resources of Mouse NeuroBehavior Core in the Institute of Comparative Medicine, Columbia University Irving Medical Center.

Competing interests

S.F.T. is a co-inventor of Emory-owned intellectual property. S.F.T. is a member of the SAB for Sage Therapeutics, Eumentis Therapeutics, Neurocrine, the GRIN2B Foundation, the CureGRIN Foundation, and CombinedBrain. S.F.T. is a consultant for GRIN Therapeutics. S.F.T. is cofounder of NeurOp, Inc. and Agrithera. T.T.S is a consultant for BioMarin Pharmaceuticals.

Supplementary material

Supplementary material is available at *Brain* online.

References

1. Hansen KB, Wollmuth LP, Bowie D, *et al*. Structure, Function, and Pharmacology of Glutamate Receptor Ion Channels. *Pharmacol Rev*. Oct 2021;73(4):298-487. doi:10.1124/pharmrev.120.000131

2. Tsien JZ. Linking Hebb's coincidence-detection to memory formation. *Curr Opin Neurobiol*. Apr 2000;10(2):266-73. doi:10.1016/s0959-4388(00)00070-2

3. Collingridge GL, Volianskis A, Bannister N, *et al*. The NMDA receptor as a target for cognitive enhancement. *Neuropharmacology*. Jan 2013;64:13-26. doi:10.1016/j.neuropharm.2012.06.051

4. Gambrill AC, Barria A. NMDA receptor subunit composition controls synaptogenesis and synapse stabilization. *Proc Natl Acad Sci U S A*. Apr 5 2011;108(14):5855-60. doi:10.1073/pnas.1012676108

5. Li F, Tsien JZ. Memory and the NMDA receptors. *N Engl J Med*. Jul 16 2009;361(3):302-3. doi:10.1056/NEJMcibr0902052

6. Benke TA, Park K, Krey I, *et al*. Clinical and therapeutic significance of genetic variation in the GRIN gene family encoding NMDARs. *Neuropharmacology*. Nov 1 2021;199:108805. doi:10.1016/j.neuropharm.2021.108805

7. Camp CR, Yuan H. GRIN2D/GluN2D NMDA receptor: Unique features and its contribution to pediatric developmental and epileptic encephalopathy. *Eur J Paediatr Neurol*. Jan 2020;24:89-99. doi:10.1016/j.ejpn.2019.12.007

8. XiangWei W, Kannan V, Xu Y, *et al*. Heterogeneous clinical and functional features of GRIN2D-related developmental and epileptic encephalopathy. *Brain*. Oct 1 2019;142(10):3009-3027. doi:10.1093/brain/awz232

9. Li D, Yuan H, Ortiz-Gonzalez XR, *et al*. GRIN2D Recurrent De Novo Dominant Mutation Causes a Severe Epileptic Encephalopathy Treatable with NMDA Receptor Channel Blockers. *Am J Hum Genet*. Oct 6 2016;99(4):802-816. doi:10.1016/j.ajhg.2016.07.013

10. Platzer K, Krey I, Lemke JR. GRIN2D-Related Developmental and Epileptic Encephalopathy. In: Adam MP, Mirzaa GM, Pagon RA, *et al*, eds. *GeneReviews((R))*. 2022.

11. von Engelhardt J, Bocklisch C, Tonges L, Herb A, Mishina M, Monyer H. GluN2D-containing NMDA receptors-mediate synaptic currents in hippocampal interneurons and pyramidal cells in juvenile mice. *Front Cell Neurosci*. 2015;9:95. doi:10.3389/fncel.2015.00095

12. Hanson E, Armbruster M, Lau LA, *et al*. Tonic Activation of GluN2C/GluN2D-Containing NMDA Receptors by Ambient Glutamate Facilitates Cortical Interneuron Maturation. *J Neurosci*. May 8 2019;39(19):3611-3626. doi:10.1523/JNEUROSCI.1392-18.2019

13. Perszyk RE, DiRaddo JO, Strong KL, *et al*. GluN2D-Containing N-methyl-d-Aspartate Receptors Mediate Synaptic Transmission in Hippocampal Interneurons and Regulate Interneuron Activity. *Mol Pharmacol*. Dec 2016;90(6):689-702. doi:10.1124/mol.116.105130

14. Kirson ED, Schirra C, Konnerth A, Yaari Y. Early postnatal switch in magnesium sensitivity of NMDA receptors in rat CA1 pyramidal cells. *J Physiol*. Nov 15 1999;521 Pt 1(Pt 1):99-111. doi:10.1111/j.1469-7793.1999.00099.x

15. Scherzer CR, Landwehrmeyer GB, Kerner JA, *et al*. Expression of N-methyl-D-aspartate receptor subunit mRNAs in the human brain: hippocampus and cortex. *J Comp Neurol*. Jan 5 1998;390(1):75-90. doi:10.1002/(sici)1096-9861(19980105)390:1<75::aid-cne7>3.0.co;2-n

16. Akazawa C, Shigemoto R, Bessho Y, Nakanishi S, Mizuno N. Differential expression of five N-methyl-D-aspartate receptor subunit mRNAs in the cerebellum of developing and adult rats. *J Comp Neurol*. Sep 1 1994;347(1):150-60. doi:10.1002/cne.903470112

17. Monyer H, Burnashev N, Laurie DJ, Sakmann B, Seeburg PH. Developmental and regional expression in the rat brain and functional properties of four NMDA receptors. *Neuron*. Mar 1994;12(3):529-40. doi:10.1016/0896-6273(94)90210-0

18. Potworowski J, Jakuczun W, Leski S, Wojcik D. Kernel current source density method. *Neural Comput*. Feb 2012;24(2):541-75. doi:10.1162/NECO_a_00236

19. Boudreau RL, Garwick-Coppens SE, Liu J, Wallace LM, Harper SQ. Rapid Cloning and Validation of MicroRNA Shuttle Vectors: A Practical Guide. In: Harper SQ, ed. *RNA Interference Techniques*. Humana Press; 2011:19-37.

20. Wallace LM, Saad NY, Pyne NK, *et al.* Pre-clinical Safety and Off-Target Studies to Support Translation of AAV-Mediated RNAi Therapy for FSHD. *Mol Ther Methods Clin Dev.* Mar 16 2018;8:121-130. doi:10.1016/j.omtm.2017.12.005

21. Wallace LM, Liu J, Domire JS, *et al.* RNA interference inhibits DUX4-induced muscle toxicity in vivo: implications for a targeted FSHD therapy. *Mol Ther*. Jul 2012;20(7):1417-23. doi:10.1038/mt.2012.68

22. Raina A, Ferrante F, Bisol A, Fiori G, Galeone M. Cardiotoxicity during chemotherapy for advanced gastroenteric tumors. *Tumori.* Aug 31 1987;73(4):359-61. doi:10.1177/030089168707300407

23. Yerger J, Cougnoux AC, Abbott CB, *et al.* Phenotype assessment for neurodegenerative murine models with ataxia and application to Niemann-Pick disease, type C1. *Biol Open*. Apr 15 2022;11(4)doi:10.1242/bio.059052

24. Singec I, Knoth R, Vida I, Frotscher M. The rostral migratory stream generates hippocampal CA1 pyramidal-like neurons in a novel organotypic slice co-culture model. *Biol Open*. Sep 4 2015;4(10):1222-8. doi:10.1242/bio.012096

25. Turner KL, Sontheimer H. KCa3.1 modulates neuroblast migration along the rostral migratory stream (RMS) in vivo. *Cereb Cortex*. Sep 2014;24(9):2388-400. doi:10.1093/cercor/bht090

26. Lalonde R, Strazielle C. Brain regions and genes affecting limb-clasping responses. *Brain Res Rev*. Jun 24 2011;67(1-2):252-9. doi:10.1016/j.brainresrev.2011.02.005

27. Jafarian M, Esmaeil Alipour M, Karimzadeh F. Experimental Models of Absence Epilepsy. *Basic Clin Neurosci.* Nov-Dec 2020;11(6):715-726. doi:10.32598/bcn.11.6.731.1

28. Pearce PS, Friedman D, Lafrancois JJ, *et al.* Spike-wave discharges in adult Sprague-Dawley rats and their implications for animal models of temporal lobe epilepsy. *Epilepsy Behav*. Mar 2014;32:121-31. doi:10.1016/j.yebeh.2014.01.004

29. Swanger SA, Vance KM, Pare JF, *et al.* NMDA Receptors Containing the GluN2D Subunit Control Neuronal Function in the Subthalamic Nucleus. *J Neurosci.* Dec 2 2015;35(48):15971-83. doi:10.1523/JNEUROSCI.1702-15.2015

30. Ziburkus J, Cressman JR, Schiff SJ. Seizures as imbalanced up states: excitatory and inhibitory conductances during seizure-like events. *Journal of neurophysiology*. Mar 2013;109(5):1296-306. doi:10.1152/jn.00232.2012

31. Wehr M, Zador AM. Balanced inhibition underlies tuning and sharpens spike timing in auditory cortex. *Nature*. Nov 27 2003;426(6965):442-6. doi:10.1038/nature02116

32. Glasgow SD, McPhedrain R, Madranges JF, Kennedy TE, Ruthazer ES. Approaches and Limitations in the Investigation of Synaptic Transmission and Plasticity. *Front Synaptic Neurosci*. 2019;11:20. doi:10.3389/fnsyn.2019.00020

33. Louiset E, Valentijn JA, Vaudry H, Cazin L. Central-type benzodiazepines modulate GABAA receptor chloride channels in cultured pituitary melanotrophs. *Brain Res Mol Brain Res*. Jan 1992;12(1-3):1-6. doi:10.1016/0169-328x(92)90062-g

34. Aimiuwu OV, Fowler AM, Sah M, *et al.* RNAi-Based Gene Therapy Rescues Developmental and Epileptic Encephalopathy in a Genetic Mouse Model. *Mol Ther*. Jul 8 2020;28(7):1706-1716. doi:10.1016/j.ymthe.2020.04.007

35. Ikeda K, Araki K, Takayama C, *et al.* Reduced spontaneous activity of mice defective in the epsilon 4 subunit of the NMDA receptor channel. *Brain Res Mol Brain Res*. Oct 1995;33(1):61-71. doi:10.1016/0169-328x(95)00107-4

36. Tsuchida N, Hamada K, Shiina M, *et al.* GRIN2D variants in three cases of developmental and epileptic encephalopathy. *Clin Genet.* Dec 2018;94(6):538-547. doi:10.1111/cge.13454

37. Tyzio R, Holmes GL, Ben-Ari Y, Khazipov R. Timing of the developmental switch in GABA(A) mediated signaling from excitation to inhibition in CA3 rat hippocampus using gramicidin perforated patch and extracellular recordings. *Epilepsia*. 2007;48 Suppl 5:96-105. doi:10.1111/j.1528-1167.2007.01295.x

38. Lim L, Mi D, Llorca A, Marin O. Development and Functional Diversification of Cortical Interneurons. *Neuron*. Oct 24 2018;100(2):294-313. doi:10.1016/j.neuron.2018.10.009

39. Mao Z, He S, Mesnard C, *et al.* NMDA receptors containing GluN2C and GluN2D subunits have opposing roles in modulating neuronal oscillations; potential mechanism for bidirectional feedback. *Brain Res*. Jan 15 2020;1727:146571. doi:10.1016/j.brainres.2019.146571

40. Chen QY, Li XH, Lu JS, *et al.* NMDA GluN2C/2D receptors contribute to synaptic regulation and plasticity in the anterior cingulate cortex of adult mice. *Mol Brain*. Mar 25 2021;14(1):60. doi:10.1186/s13041-021-00744-3

41. Sjostedt E, Zhong W, Fagerberg L, *et al.* An atlas of the protein-coding genes in the human, pig, and mouse brain. *Science*. Mar 6 2020;367(6482)doi:10.1126/science.aay5947

42. Ogiwara I, Iwasato T, Miyamoto H, *et al.* Nav1.1 haploinsufficiency in excitatory neurons ameliorates seizure-associated sudden death in a mouse model of Dravet syndrome. *Hum Mol Genet.* Dec 1 2013;22(23):4784-804. doi:10.1093/hmg/ddt331

43. Doyle S, Hansen DB, Vella J, *et al.* Vesicular glutamate release from central axons contributes to myelin damage. *Nat Commun*. Mar 12 2018;9(1):1032. doi:10.1038/s41467-018-03427-1

44. Luo T, Wu WH, Chen BS. NMDA receptor signaling: death or survival? *Front Biol (Beijing)*. Dec 2011;6(6):468-476. doi:10.1007/s11515-011-1187-6

45. Makinson CD, Tanaka BS, Sorokin JM, *et al.* Regulation of Thalamic and Cortical Network Synchrony by Scn8a. *Neuron*. Mar 8 2017;93(5):1165-1179 e6. doi:10.1016/j.neuron.2017.01.031

46. Kvajo M, McKellar H, Drew LJ, *et al.* Altered axonal targeting and short-term plasticity in the hippocampus of Disc1 mutant mice. *Proc Natl Acad Sci U S A*. Dec 6 2011;108(49):E1349-58. doi:10.1073/pnas.1114113108

47. Wang W, Frankel WN. Overlaps, gaps, and complexities of mouse models of Developmental and Epileptic Encephalopathy. *Neurobiol Dis*. Jan 2021;148:105220. doi:10.1016/j.nbd.2020.105220

Figure legends

Figure 1 Modeling and validation of *Grin2d* V664I phenotypes in mouse. (A) Oligonucleotide-directed CRISPR mutagenesis replaced CG with AA, resulting in the orthologous *Grin2d* V664I mutation in constitutive Grin2d V664I mice, corresponding to patients' *GRIN2D* V667I mutation. **(B)** Onset of hindlimb clasping in *Grin2d* V664I/+ pups occurred around P13-P15. The probability of hindlimb clasping for each genotype at P31 are shown. WT, N= 8; *Grin2d*+/-(cKI), N=15; OT V664I/+, N=29; *Sox2-Cre* V664I/+, N=15, Kruskal-Wallis test, significance indicated at *P*<0.0001****. **(C)** *Grin2d* V664I/+ pups weighed less than control littermates. *P*<0.0001 repeated measures ANOVA with litter origin and sex as covariates; +/+, N=17; V664I/+, N=14. **(D)** *Grin2d* V664I/+ pups have fewer separation-induced vocalizations than +/+ littermates at all ages tested. +/+, N=14; V664I/+, N=13. Data were compared using the non-parametric two-tailed Wilcoxon rank-sum test at each age. **(E)** H&E-stained brain sections at P7 and P14. Black dotted arrows (same length, 3mm) indicate consistent visual comparisons of smaller thalamus, hypothalamus, striatum and cerebellum in *Grin2d* V664I pups at P7 and P14. +/+: N=3; V664I/+: N=3 at each age. Scale bars, 1 mm. **(F)** A conditional knock-in (cKI) cassette was inserted between exon 7 and 8 to generate *Grin2d* V664I cKI mice. Our knockout-first strategy utilizes LoxP-SV40/pA3X-LoxP to inactivate gene expression until *Cre* recombination occurs. **(G)** Western blot of GluN2D expression in the forebrain and **(H)** quantification based on band intensity. +/+, N=4; *Sox2-Cre Grin2d* V664I/+: N=4; *Grin2d*$^{+/-}$: N=4. **(I)** Survival curves for constitutive *Grin2d* V664I/+ (OT), V664I/+ *Sox2-Cre*, *Grin2d*+/+ (WT) and *Grin2d*+/-(cKI). All *Grin2d*+/+ (WT) and *Grin2d*+/-(cKI) mice survived to P60 (*Grin2d*+/+, N=11; Grin2d+/-, N=13. Log rank test, not significant, *P*>0.05). Therefore, *Grin2d*+/+ (WT) and *Grin2d*+/-(cKI) are grouped as controls in subsequent test. OT vs controls, *P*=5.2e-8***; V664I/+ *Sox2-Cre* vs controls, *P*=0.006**. Controls (*Grin2d*+/- and +/+), N= 24; OT V664I/+, N= 25; cKI *Sox2-Cre* V664I/+, N= 22. **(J)** Survival curves for V664I/+ *Gad2-Cre*, *Gad2/Emx1* double-*Cre*. V664I/+ *Gad2-Cre* vs controls, *P*=6.66e-16***; *Gad2/Emx1* double-*Cre* vs controls, *P*=0.00001***. Controls (*Cre*+/-), N= 9; cKI, *Gad2-Cre* V664I/+, N= 19. Survival data were tested pairwise log-rank test. All *Pvalb-Cre*, *Emx1-Cre* and *Sst-Cre* mutants survived up to P60, thus their survival curves were not shown here. **(K & L)** Cleaved caspase-3 staining and cell death quantification at P16 show increased cell death in the RMS and hippocampus of V664I/+ *Gad2-Cre* mice, but not in *Emx1-Cre* and *Sox2-Cre*

mice. Enlarged inset i-iv shows cleaved Caspase-3 cells in the RMS. Controls, N= 4; *Sox2-Cre* V664I/+, N=3, *Gad2-Cre* V664I/+, N= 8; *Emx1-Cre* V664I/+, N=4, Mann-Whiteney test, significance indicated at $P<0.05$*, $P<0.01$**. Scale bars, 500 µm.

Figure 2 EEG of *Grin2d* cKI mice. Representative EEG traces for **(A)** Wildtype or *Grin2d*$^{+/-}$ (controls) mice and **(B)** OT V664/+ or *Sox2-Cre* V664I/+ mutants at two temporal resolutions (upper and middle panels). **(C)** Lethal seizure, marked by red dotted line, were captured from *Sox2-Cre* V664I/+ mice. **(D)** EEG traces from *Pvalb-Cre* V664I/+ mice. Insets showed zoomed EEG traces. FR, right and FL, left anterior electrodes were referenced to a cerebellar electrode as described in Methods. **(E)** Averaged power spectra plotted as moving average, and **(F)** shows cumulative plots for each of three frequency sub-ranges: 1 Hz-4 Hz, 4 Hz–7 Hz, 7 Hz–10 Hz. Non-parametric pairwise analyses for these ranges are given on **Table S1**.

Figure 3 Heterogeneity of SWD-like activity in *Sox2-Cre* and *Pvalb-Cre* V664/+ mice and the onset of seizure in *Sox2-Cre* V664I/+ mice. (A) Representative EEG trace of each of SWD event type categorized as to whether ongoing locomotor activity was arrested during the event or continued. 8.7 Hz ± 0.58 SE no arrest; vs. 6.7 Hz ± 0.08 SE arrest, $P=2 \times 10^{-10}$, Kruskal-Wallis nonparametric test. **(B)** Average fundamental frequency (top) and average duration (bottom) of SWD events determined from four mice of each genotype. *Sox2-Cre* arrest: 20.3 s ± 2.1 SE; *Sox2-Cre* no arrest: 8.3 s ± 0.06; $P=2 \times 10^{-13}$, Kruskal-Wallis nonparametric test; *Pvalb-Cre*: 23.3 s ± 1.9 SE. Colors represent individual mice within each mouse line. $P<0.0001$****, ns, not significant. **(C)** A micrographic depiction illustrating the arrangement of electrodes and perforations within a section of the NeuroGrid device, accompanied by a representative image highlighting the barrel cortex where the electrodes are surgically implanted (white dotted box). **(D)** Representative cortical activities from WT and V664I/+ recorded at P6-P7 and **(E)** P13-P14 are shown. Inset i-iv highlighted sleep spindles (blue) and epileptic bursts (purple) from selected channels. P6-P7, +/+, N= 4, V664/+, N= 4; P13-P14, +/+, N= 4, V664/+, N= 4.

Figure 4 Synaptic abnormalities in V664I/+ mice. (A) Synaptic clumps in *Grin2d* V664I (white arrowheads) and synaptic counts of **(B)** small (<1 µm) and **(C)** large (>2.5 µm) synapses. Mann-Whitney test, significance indicated at $P<0.05$* and $P<0.001$***, Controls, N=4 animals, n=14 neurons; *Sox2-Cre* V664I/+, N=5 animals, n=18 neurons. Scale bars, 20 µm. **(D)** STORM images of single synapse from controls and *Sox2-Cre* V664I/+ primary hippocampal neurons and **(E)** quantification of presynapse, postsynapse sizes and the distance between synaptic cleft. Controls, N=7 animals, n=61 synapses; *Sox2-Cre* V664I/+, N=6 animals, n=86 synapses. Shapiro-Wilk test, followed by Welch's t-test, significance indicated at $P<0.05$* and $P<0.01$**. Scale bars, 0.2 µm. **(F)** Synaptic clumps were seen in *Grin2d* V664I hippocampal CA3 (i) stratum pyramidale layer together with a reduction of synaptic vesicles in CA1 (ii) SR layer. Quantification of synaptophysin puncta larger than 3.5 µm in **(G)** CA3 and **(H)** CA1 across hippocampal SR, SP and SO layers. Welch's t-test, significance indicated at $P<0.05$*, Controls, N=3; *Sox2-Cre* V664I/+, N=3. Scale bars, 500 µm.

Figure 5 Synaptic dysfunction in the V664I/+ hippocampus. (A) Representative evoked NMDA receptor currents recorded from CA1 excitatory and inhibitory neurons. No significant difference in weighted-Tau was observed in Grin2d V664I/+ mutant mice compared to controls. Mann-Whitney test. Excitatory neurons: Controls, N=3 animals, n=5 cells/animal; V664I/+, N=3 animals, n=5 cells/animal. Inhibitory neurons: Controls, N=4 animals, n=10 cells/animal; V664I/+, N=3 animals, n=14 cells/animal. **(B)** Cumulative histogram plots sIPSC inter-event interval and amplitude show a significant leftward shift in Grin2d V664I/+ mutants, indicating increased inhibitory synaptic activity. Kolmogorov-Smirnov test, $P<0.001$***. N=4 animals, n=14 cells/animal per genotype. **(C)** The mIPSC inter-event interval is significantly shifted to the left in *Grin2d* V664I/+ mutant mice, while mIPSC amplitude is unchanged. Kolmogorov-Smirnov test, significance indicated at $P<0.001$***. N=4 mice, n=14 cells/mice for each genotype.

Figure 6 Circuit dysfunction in the V664I/+ hippocampus. (A) Diagram of the experimental setup depicting hippocampal-entorhinal cortex (HEC) slice preparation**. (B)** Average surface CSD plot of control and V664I/+ mice up to 0.05s post stimulation are shown. Upper right inset shows flatten 2D-plot. **(C)** Quantification of current volume, dispersion and minima. Two-tailed Mann

Whitney test, significant at $P<0.01$** and $P<0.001$***. Current volumes, V664I/+: 6.50 ± 0.66 s·A/mm^2, +/+: 3.12 ± 0.37 s·A/mm^2, $P= 4.8 \times 10^{-5}$***; smaller minima, V664I/+: -24.87 ± 2.34 µA/mm^3, +/+: -13.86 ± 1.99 µA/mm^3, $P= 0.003$**; dispersion, V664I/+: 120.13 ± 9.61 A/mm^3, +/+: 48.81 ± 5.22 A/mm^3, $P= 1.6 \times 10^{-6}$***. Recordings were repeated after addition of 200nM clonazepam. **(D)** Average surface CSD plot of control and V664I/+ mice up to 0.05s post stimulation are shown with flatten 2D-plot embedded on top right. **(E)** The percentage of current volume change from baseline (without clonazepam), dispersion and current minima are shown. Two-tailed Mann Whitney test, significant at $P<0.001$***. Current volume, mutant: 7.43 ± 0.55 s·A/mm^2, +/+: 1.33 ± 0.38 s·A/mm^2, P=2.4285e-8; minima, V664I/+: -28.96 ± 1.77 µA/mm^3, +/+: -5.86 ± 1.81 µA/mm^3, P=2.1000e-7; weighted dispersion, V664I/+: 146.99 ± 9.68 A/mm^3, +/+: 18.66 ± 4.81 A/mm^3, P=1.3842e-8. **(F)** Raster plots showing spike densities (50 x 1 ms bins) within the first 50 ms post electrical stimulation (left of dotted red line) and 50 – 200 ms (right of dotted red line). Data from 5 sweeps (trial #) of stimulation for each of 5 mice sampled per genotype are shown. **(G)** Spike frequency and **(H)** spike counts for untreated slices. The same recording was repeated with clonazepam 200 nM and **(I)** the raster plot of the first 50 ms and 50-200 ms, separated by a red dotted line is shown. Quantifications for **(J)** spike frequency and **(K)** spikes counts. Two-tailed Mann Whitney test, significant at $P<0.01$** and $P<0.001$***.

Figure 7 RNAi treatment reduces V664I seizure burden. (A) Screening five mi*Grin2d* candidates via luciferase assay in HEK-293 cells identified mi*Grin2d*-791 as the most effective, with a knockdown rate of 61%, Each candidate was tested nine times in three separate repeats. Mann-Whitney test, significance indicated at $P<0.001$*** and $P<0.0001$****. **(B)** *Grin2d* RNA knockdown rate by different doses of mi-791. **(C)** Averaged power spectra plotted as moving average, and **(D)** shows cumulative plots for each of three frequency sub-ranges: 1 Hz-4 Hz, 4 Hz–7 Hz, 7 Hz–10 Hz. Non-parametric pairwise analyses for these ranges are given on **Table S2**. **(E)** Representative SWDs from untreated and mi*Grin2d*-791-treated (mid dose) mice. **(F)** Scatter plot for SWDs duration and frequency. Comparison of **(G)** seizure burden, **(H)** average SWD length. Mann Whitney test, significant at $P<0.05$*, $P<0.01$** and $P<0.001$***.

Table 1 Age and the number of mice subjected to vEEG recording

Grin2d Genotype	Age range (days)	Average hours of continuous recording	Number of mice with SWD-like activity/total[a]	Number of terminal TCS captured
OT, V664I/+ (N=29)	17–20	49.1	5/5	1
	20–30	46.3	6/7	–
	30–40	45.8	21/21	3
	41–80	45.0	10/10	–
OT, +/+ (N=8)	24–38	47.9	0/8	–
cKI, *Sox2-Cre* V664I/+ (N=18)	20–30	42.7	6/6	–
	30–40	47.6	8/8	–
	40–60	47.7	6/6	–
	60–70	48.4	8/8	1
cKI, +/+ or no Sox2-cre (N=10)	23–49	46.8	0/10	–

The number of mice and their ages at vEEG recording are shown above.

[a]Individual mice were recorded at multiple ages.

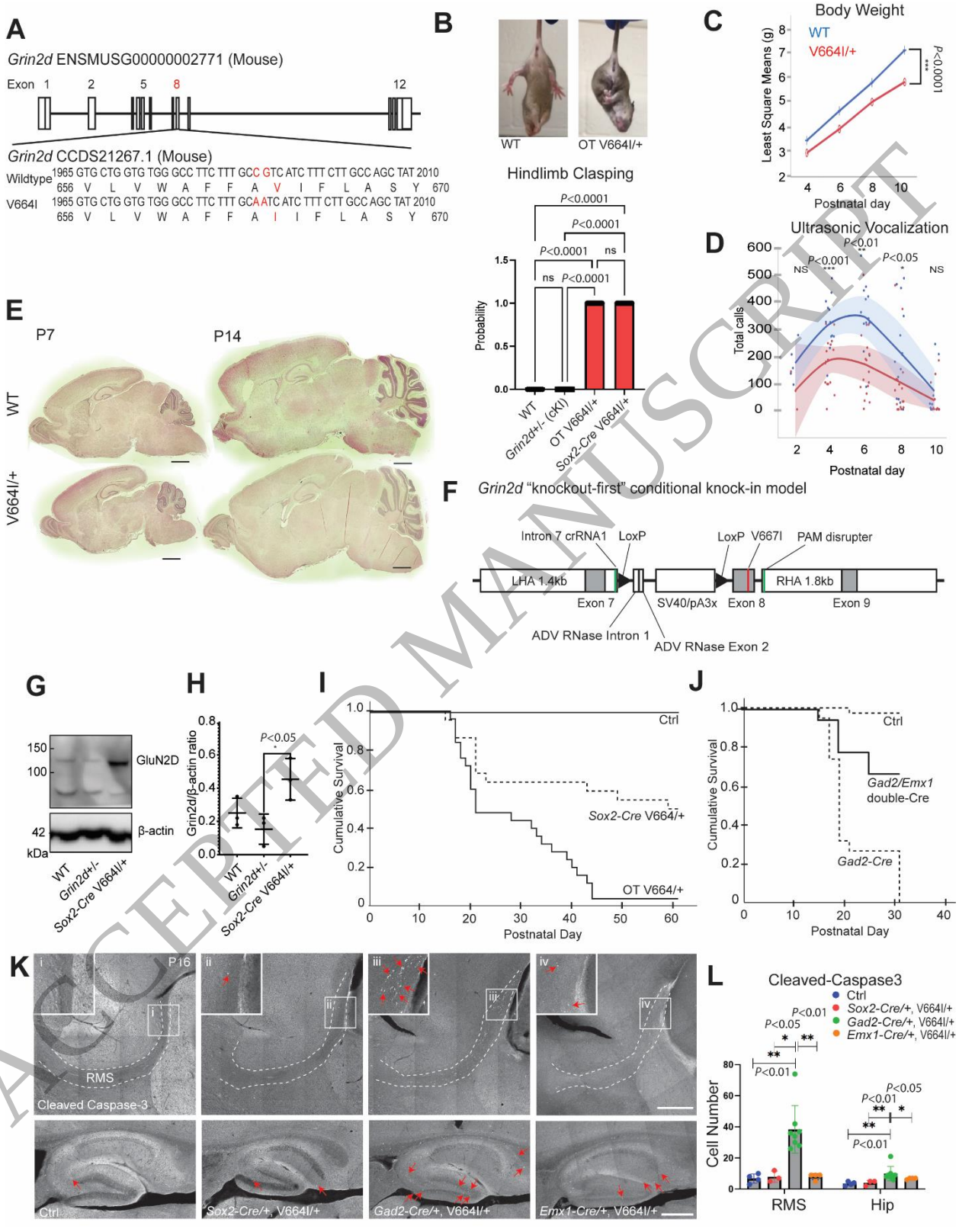

Figure 1
213x274 mm (DPI)

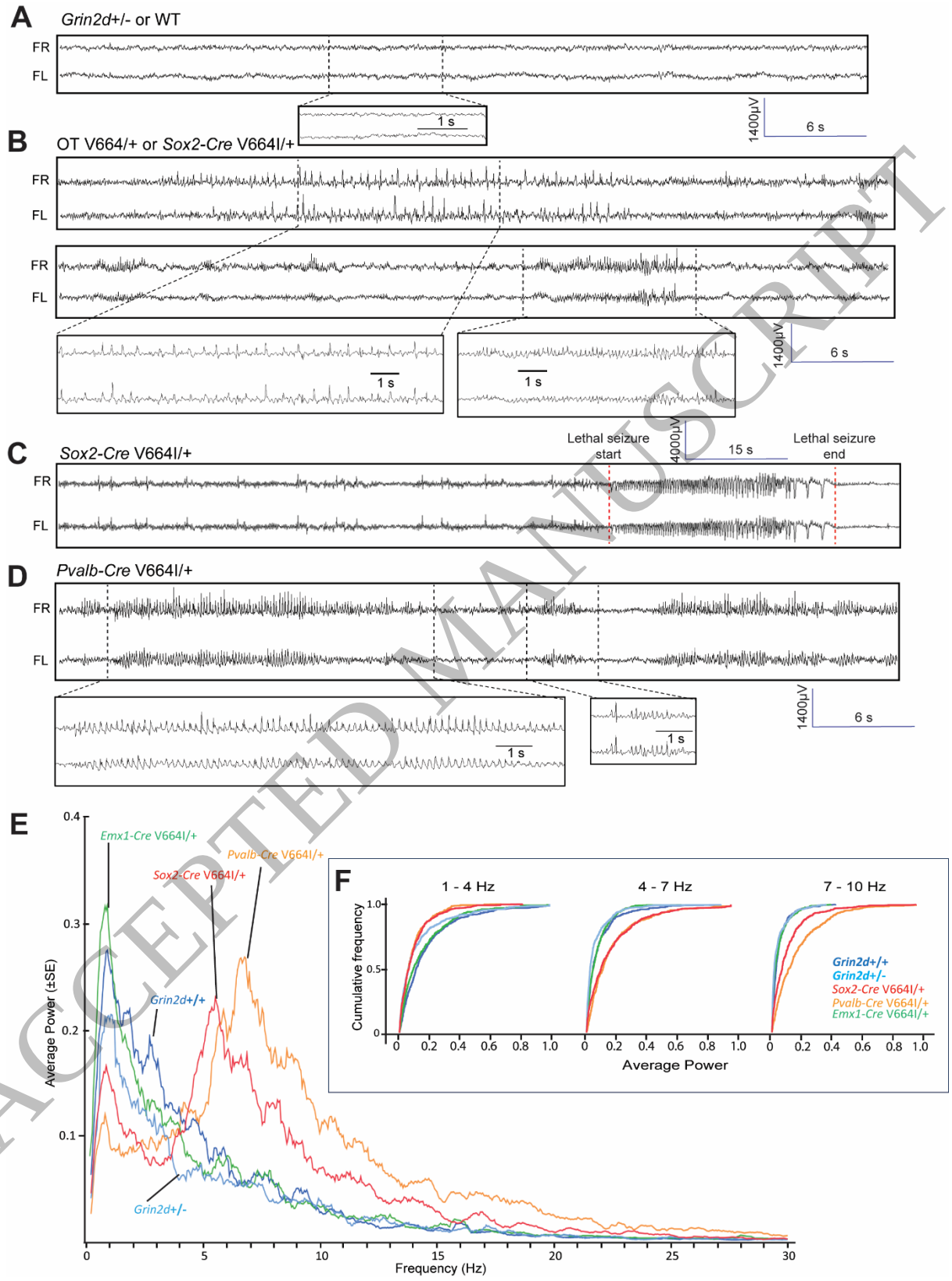

Figure 2
201x272 mm (DPI)

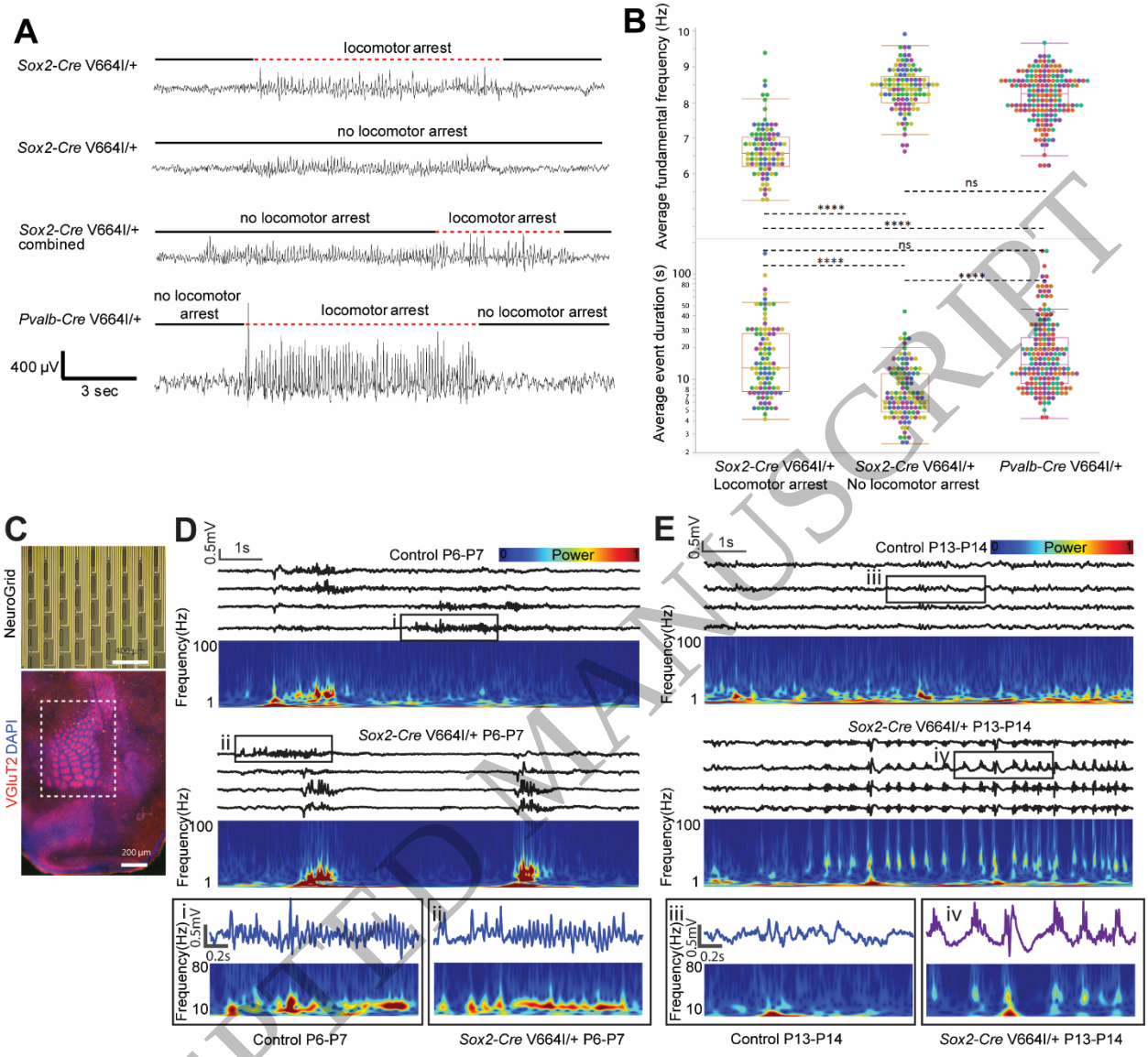

Figure 3
214x196 mm (DPI)

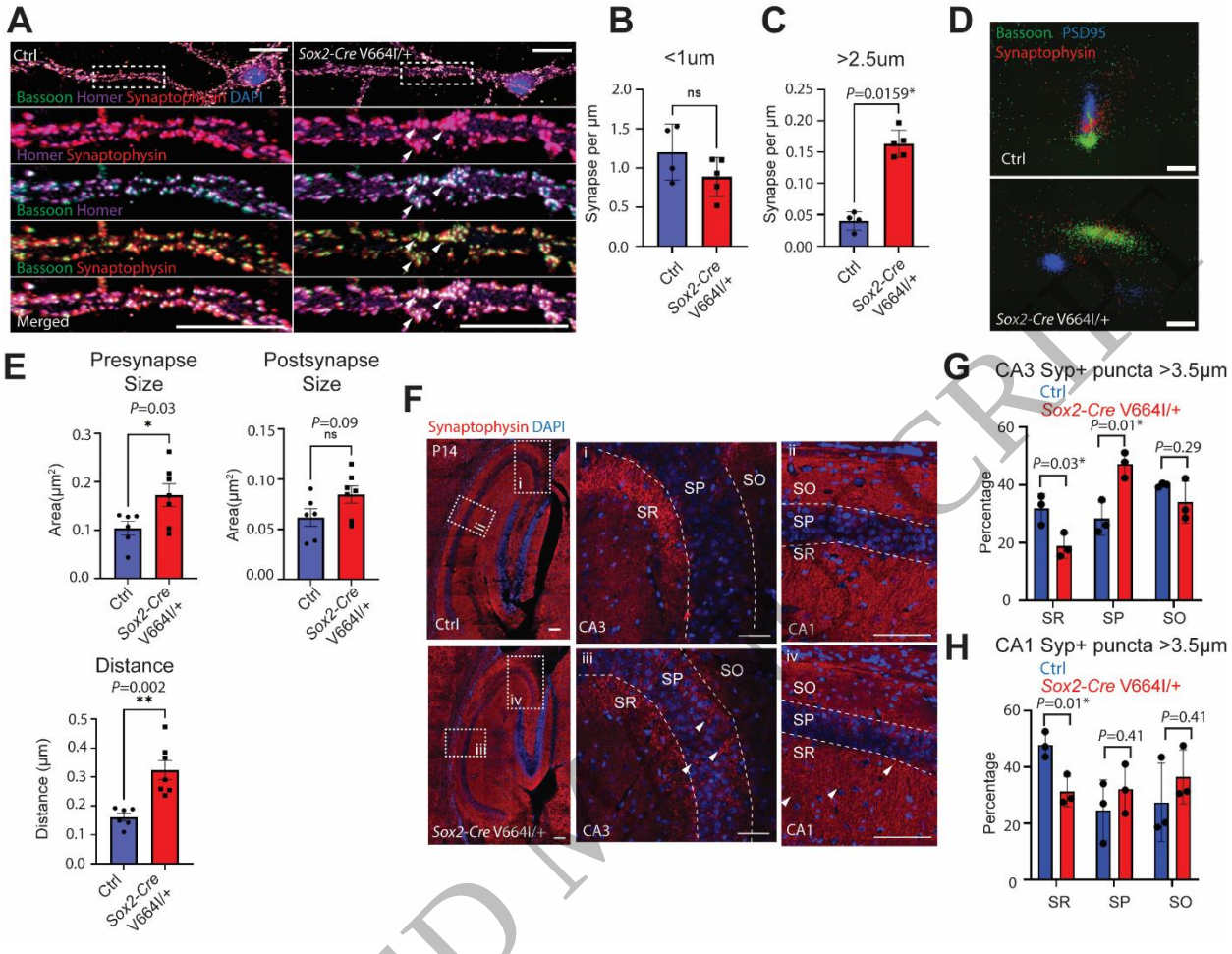

Figure 4
213x164 mm (DPI)

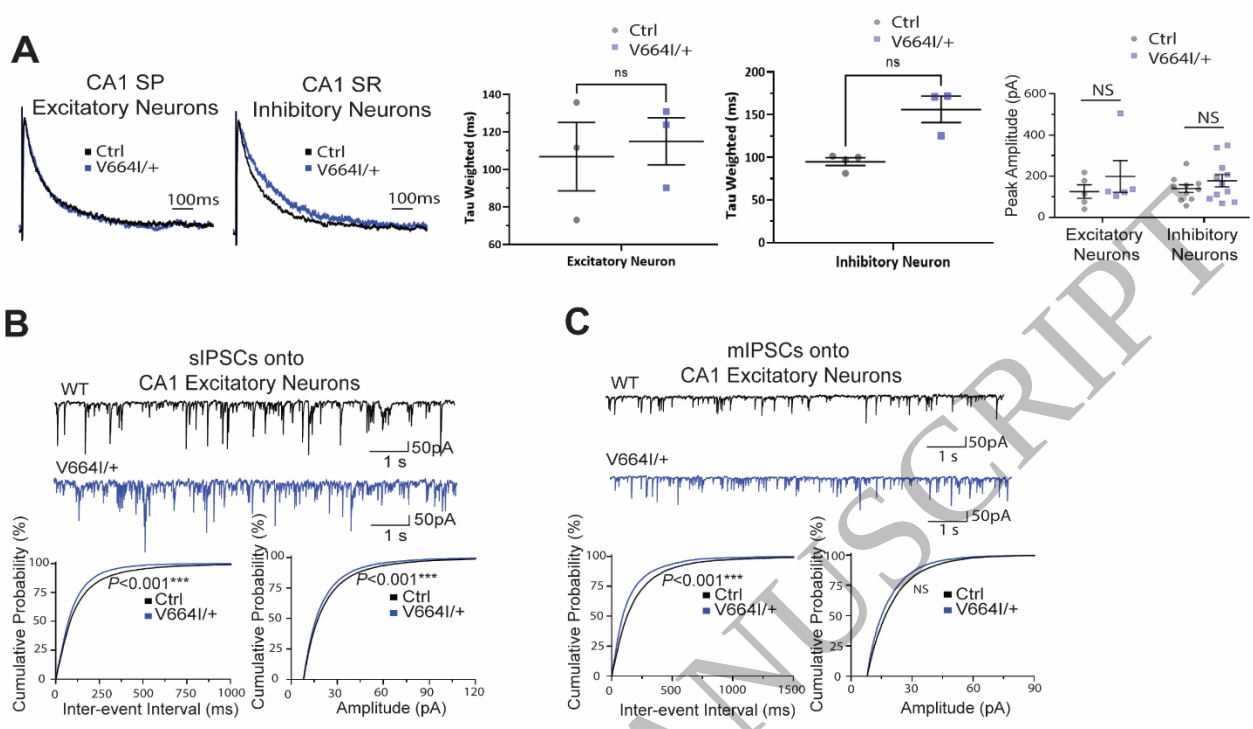

Figure 5
212x122 mm (DPI)

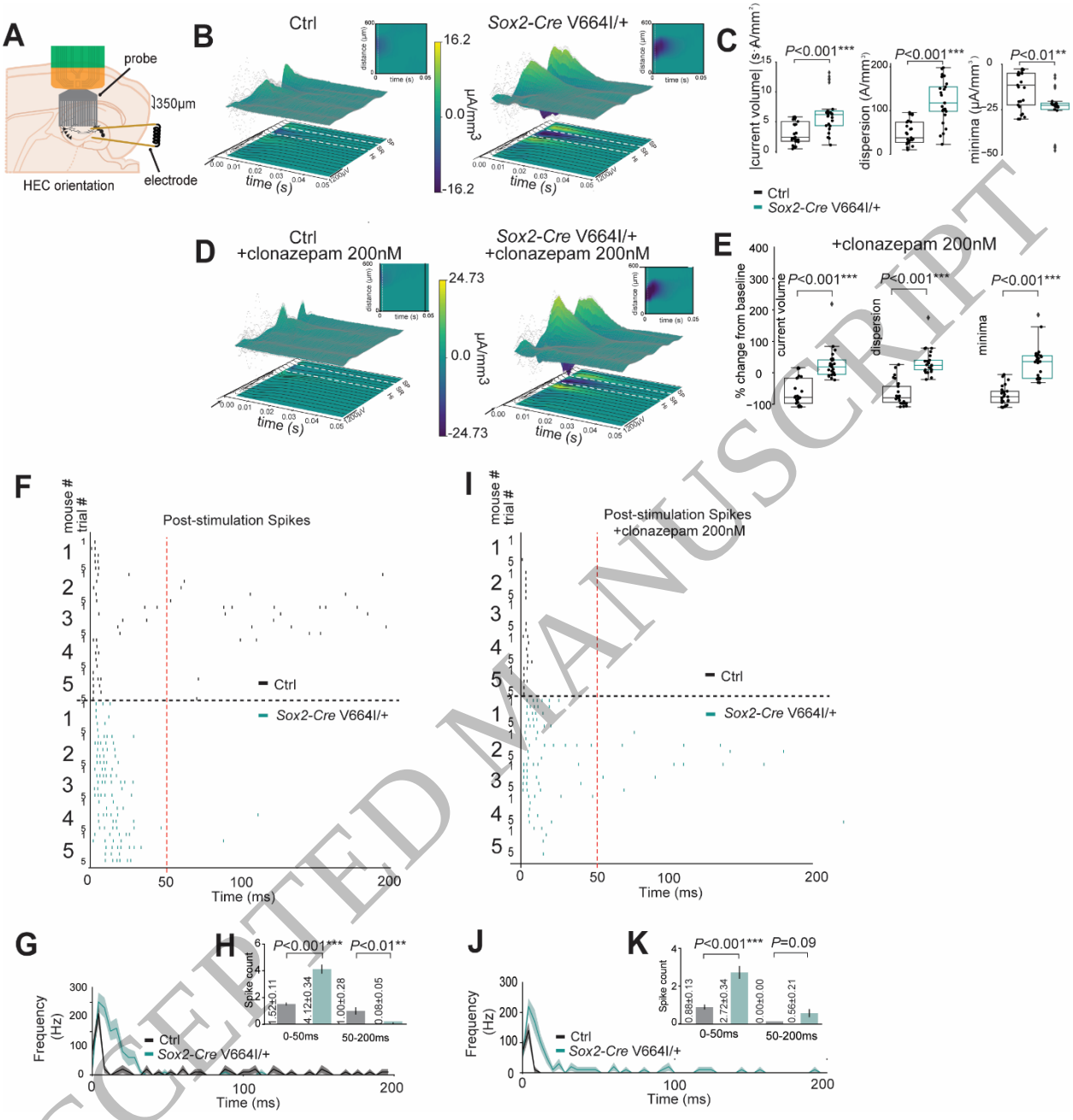

Figure 6
212x220 mm (DPI)

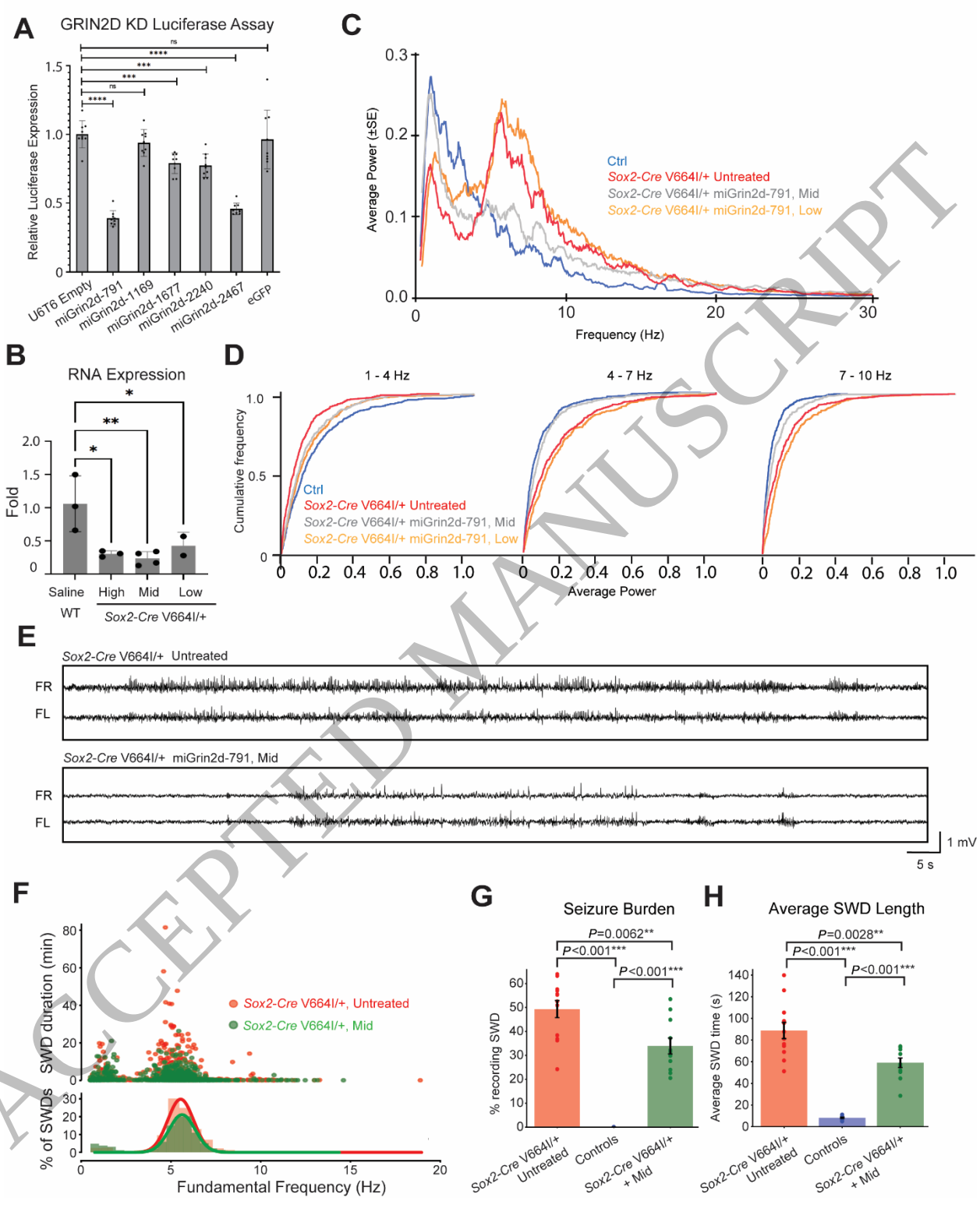

Figure 7
213x263 mm (DPI)